Spring 5-3-2011

DEM-CFD Modeling of a Bubbling Fluidized Bed and a Wurster Coater

Lennart Fries
Hamburg University of Technology, lennart.fries@tuhh.de

Sergiy Antonyuk
Hamburg University of Technology, antonyuk@tuhh.de

Stefan Heinrich
Hamburg University of Technology, stefan.heinrich@tuhh.de

Stefan Palzer
Nestec SA, Switzerland

DEM-CFD MODELING OF A TOP-SPRAY FLUIDIZED BED GRANULATOR AND A WURSTER-COATER

Lennart Fries[1], Sergiy Antonyuk[1], Stefan Heinrich[1] and Stefan Palzer[2]

[1] Institute of Solids Process Engineering and Particle Technology,
Hamburg University of Technology
Denickestr. 15, 21073 Hamburg, Germany
T:+49-40-42878 2143; F:+49-40-42878-2678; E: lennart.fries@tuhh.de

[2] Nestlé Product Technology Centre York,
Haxby Road, York YO91 1XY, United Kingdom

ABSTRACT

Coupled DEM-CFD simulations were performed to study the fluid and particle dynamics of a fluidized bed granulator on the micro-scale. In a first study, wetting of the particles is estimated based on the residence time distribution inside a conical spray zone. The effect of the geometry of the apparatus on the homogeneity of wetting is analyzed in order to understand the performance and specificity of different granulator configurations. For a small simulation system, heat and mass transfer laws were resolved to calculate the moisture content of the individual particles An effective modelling tool for design of a fluidized bed spray granulator is obtained.

INTRODUCTION

Fluidized bed spray granulation plays an important role in the manufacturing of powder granules in the food and pharmaceutical industries as it allows producing dust-free and free-flowing particles.
Liquid binder is sprayed into a bed of solids to achieve granule growth. A homogeneous distribution of the spray liquid is a prerequisite for uniform growth, whereas local overwetting leads to the formation of particle clusters. The moisture distribution in the apparatus is a key parameter affecting both particle size and structure of the product [1]. The fluid bed granulation process is controlled by many parameters which can influence size and structure of the product. Since so far the choice of operating conditions and the design of the equipment geometry have been made empirically, the actual influence of the fundamental mechanisms in the process is not well understood.
To describe the process in detail on the scale of individual particles, the Discrete-Element-Method (DEM) offers large potential. As each particle is tracked individually, the method allows a complete representation of the particle-particle and particle-wall interactions and their influence on the process dynamics.

MATHEMATICAL MODEL

The motion of each particle i in the system is calculated using Newton's second law:

$$m_i \frac{d\mathbf{v}_i}{dt} = -V_i \nabla p + \frac{V_i \beta_{g-p}}{1-\varepsilon}\left(\mathbf{u}_g - \mathbf{v}_i\right) + m_i \mathbf{g} + \mathbf{F}_{c,i} + \mathbf{F}_{A,i} \quad (1)$$

The forces on the right hand side of Eq. 1 are respectively due to pressure gradient, drag, gravity and contact forces (i.e. due to collisions). The interphase momentum transfer coefficient $\beta_{g\text{-}p}$ is modeled by combining the Ergun equation [2] for dense regimes (gas volume fraction $\varepsilon < 0.8$) and the correlation by Wen&Yu [3] for dilute regimes ($\varepsilon \geq 0.8$). The gas is considered as continuous phase. The geometry of the apparatus is discretized in mesh cells and the flow profile is calculated using volume-averaged Navier-Stokes equations.

$$\frac{\partial}{\partial t}\left(\varepsilon \rho_g\right) + \nabla\left(\varepsilon \rho_g \mathbf{u}_g\right) = 0 \quad (2)$$

$$\frac{\partial}{\partial t}\left(\varepsilon \rho_g \mathbf{u}_g\right) + \nabla\left(\varepsilon \rho_g \mathbf{u}_g \mathbf{u}_g\right) = -\varepsilon\, \nabla p_g - \nabla\left(\varepsilon\, \boldsymbol{\tau}_g\right) - \mathbf{S}_p + \varepsilon \rho_g \mathbf{g} \quad (3)$$

Due to momentum exchange and the reduced free gas volume the particles influence the velocity profile of the gas phase. This effect is accounted for by adding a sink term $\mathbf{S}_p$ to the momentum balance, which closes the two-way-coupling. Forces between the gas and particle phase are of opposite direction and equal magnitude. The flow around particles is not fully resolved, as the size of the fluid mesh cells is 2-10 times larger than the particle diameter.

Contact forces between particles are calculated according to a contact model (Eq. 4) based on the theory developed by Hertz [4] for the normal impact. A no-slip approximation of the model by Mindlin and Deresiewicz [5] is applied for the tangential component of the contact force, as proposed by Tsuji et al. [6]. According to the Hertzian theory [4], the relation between the elastic deformation and the displacement is nonlinear, due to the elliptical pressure distribution in the circular contact area

$$\mathbf{F}_{c,n} = -k_n \cdot \delta_n^{3/2} \cdot \mathbf{n}_{ab} - \eta_n \mathbf{v}_{ab,n} \quad (4)$$

For the tangential component of the contact force $\mathbf{F}_t$ an equation analogue to Eq. 4 is used [6]. Energy dissipation is included in the model using coefficient of restitution, which is defined as the ratio of the square root of the elastic strain energy $E_{kin,r}$ released during the restitution to the impact energy, i.e the initial kinetic energy E_{kin} [7]:

$$e_n = \sqrt{\frac{E_{kin,r}}{E_{kin}}} = \frac{\left|\mathbf{v}_r\right|}{\mathbf{v}} \quad (5)$$

The coefficient of restitution can be determined experimentally with a free-fall tester.

Model of the spray zone

The spray injection is represented in the form of a conical zone starting from the nozzle tip, where the suspension is injected. All particles inside the spray zone are wetted. As a first approximation, the wetting intensity is supposed to be homogeneous in the entire

spray zone. By integrating over the particle trajectories, their residence time inside the spray zone is obtained, which allows estimating their moisture content.
In a second step, the model of the spray is refined by taking into account the distance between particle and nozzle tip and the local solids volume fraction. Particles in the spray zone are assigned to discrete levels (see Fig. 1).

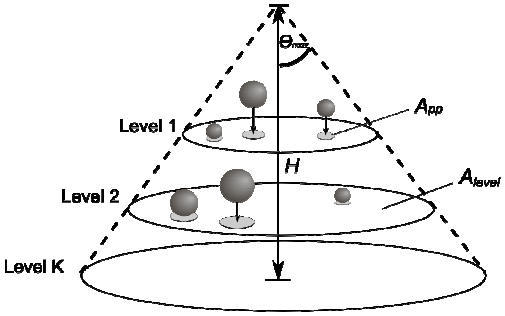

Fig. 1. Discretization scheme of the spray zone.

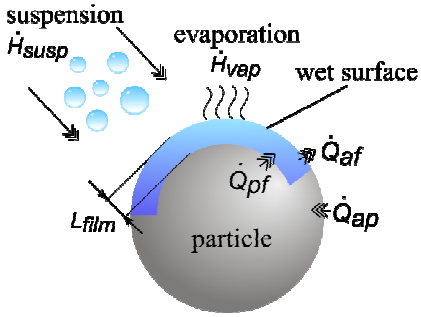

Fig. 2. Heat and enthalpy streams on the particle surface.

Starting from the nozzle tip at level j = 1, the suspension is deposited on the particles according to the ratio of the projected area of the particle to the total area of level j, according to Eq. 6. Suspension that is not deposited on level j is passed to level j+1.

$$\dot{M}_{susp,i} = \dot{M}^{j}_{susp} \cdot \frac{A_{pp,i}}{A^{j}_{level}} \tag{6}$$

$$\dot{M}^{j+1}_{susp} = \dot{M}^{j}_{susp} \cdot \left(1 - \frac{\sum A_{pp,i}}{A^{j}_{level}}\right) \tag{7}$$

Suspension, which has not been deposited until the last level of the nozzle is supposed to leave the system as overspray.

Modeling of heat and mass transfer

By applying heat and mass transfer laws, the moisture content and temperature of each individual particle can be calculated. It is assumed that suspension deposited on a particle spreads on its surface and forms a film with constant thickness L_{film} of 0.1 mm. Penetration into pores and wetting of the particle core are neglected. Deposition and evaporation of liquid influence the size of the wetted area A_{film}. If the entire particle surface is wet, it will not absorb further suspension. The enthalpy and heat streams considered in this model are shown schematically in Fig. 2. The liquid film interacts with the particle and the gas phase, which is expressed through the enthalpy balance:

$$\frac{dH_{film}}{dt} = \dot{H}_{susp} + \dot{Q}_{pf} - \dot{H}_{vap} + \dot{Q}_{af} \tag{8}$$

Evaporation of liquid will change the mass of the film. The evaporation rate depends on the mass transfer coefficient β, which is a function of the relative velocity between particle and fluid. The vapor mass flow from a particle surface is calculated:

$$\dot{M}_{vap} = \beta \cdot A_{film} \cdot \left(Y_{sat} - Y_a\right) \tag{9}$$

Heat transfer between the gas phase and the liquid film is described with the help of

$$\dot{Q}_{af} = \alpha_{af} \cdot A_{film} \cdot (\vartheta_a - \vartheta_{film}) \quad (10)$$

For dry zones on the particle surface the heat exchange between the particle and gas phase is described using

$$\dot{Q}_{ap} = \alpha_{ap} \cdot (A_p - A_{film}) \cdot (\vartheta_a - \vartheta_p) \quad (11)$$

The current contribution does not include particle growth or agglomeration.

SIMULATION CONDITIONS

In order to describe the mechanical behavior of the material (spherical γ-Al_2O_3 granules loaded with solid) the input parameters for the contact model were determined experimentally. By image analysis, the impact and rebound velocity as well as the rebound angle and the rotational speed of the particle were determined. According to results by Antonyuk et al. [7], a constant coefficient of restitution of 0.8 for γ-Al_2O_3 granules was used in the simulations. See Table 1 for all parameters of the model.

Table 1: Overview on simulation parameters.

Parameter	Value	Parameter	Value
Fluidization vel. annulus	4 m/s = $3.7 \cdot u_{mf}$	Poisson ratio	0.25
Fluidization vel. Wurster	11 m/s = $10 \cdot u_{mf}$	Static friction coeff.	0.1
Fluidization vel. top-spray	5.5 m/s = $5.1 \cdot u_{mf}$	DEM time step	$2 \cdot 10^{-6}$ s
Nozzle injection rate	7 m³/h	CFD time step	$2 \cdot 10^{-4}$ s
Fluidization air flow rate	600 m³/h	Air temperature	75 °C
Wurster gap distance	15 mm = $5 \cdot d_p$	Particle heat capacity	900 J /kgK
Normal rest. coefficient	0.8	Suspension spray rate	$5 \cdot 10^{-5}$ kg/s
Shear modulus	$1 \cdot 10^8$ Pa	Liquid film thickness	0.1 mm

For two different granulator configurations the residence time distribution of the particles inside the spray zone was analyzed. As shown in Fig. 4a, the injection nozzle can be positioned above the bubbling fluidized bed (top spray). Another common configuration is the Wurster-coater [8], where a cylindrical draft tube is inserted vertically into the granulator, as shown in Fig. 4b. Combined with a bottom-spray injection nozzle, the Wurster geometry induces a circulating movement of the particles. The draft tube physically separates the wetting zone at the center from the drying zone in the annulus.
Simulations were performed with 45,000 spherical particles and a particle diameter of 3 mm, which corresponds to a batch size of 0.95 kg at a particle density of 1500 kg/m³. The geometry of the GF5-insert used in the simulations was supplied by Glatt Ingenieurtechnik GmbH, Germany. The outer dimensions of the top-spray granulator are identical to those of the Wurster-coater. The same fluidization air flow rate and nozzle injection rate is used in both configurations. While the top-spray granulator has a homogeneous distributor plate with constant porosity, the bottom plate of the Wurster coater consists of 2 segments with different porosity. With the help of pressure drop correlations the flow rate in both segments of a Glatt GF3 insert was approximated. The nozzle injection rate in the simulations was set according to the used experimental device (Schlick type 970).

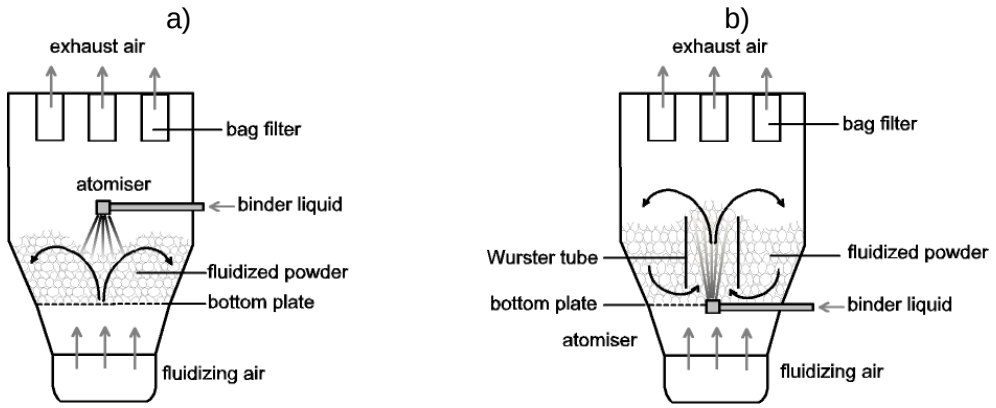

Fig. 4: Configurations of a fluidized bed granulator: (a) top-spray, (b) Wurster-coater.

For a precise investigation of particle wetting and drying in a top-spray granulator, the calculation of heat and mass transfer was coupled with the DEM-CFD simulation. Due to the higher numerical effort, a small system with 10,000 particles was analyzed, where the particle properties were identical to those given in the previous section. The simulation allows monitoring the moisture content and temperature of each individual particle. Based on the gas flow profile obtained from the CFD model, local heat and mass transfer coefficients are calculated.

SIMULATION RESULTS

The particle and fluid dynamics of both granulator configurations have been studied. In the Wurster-coater the particles move at high velocity inside the draft tube. A relatively low injection depth of the spray nozzle of approximately 45 mm was found. Obviously, the momentum of the jet is quickly transferred to the particles. In the top-spray granulator the average gas velocity is lower than in the Wurster configuration. A stagnant zone can be seen above the counter current injection nozzle.

Residence time distribution

For the Wurster-coater configuration, the residence time of the particles inside the spray zone is primarily determined by the upflow velocity of gas and particles in the draft tube. Once a stable circulating regime is established, the particles are transported through the spray zone at constantly high velocity (driven by the spout), which corresponds to a well-defined residence time and homogeneous wetting of the particles. For the given process conditions the residence time distribution obtained after 5 s simulation time is shown in Fig. 5. A clear peak at 22 ms for particles which have passed once through the spray zone and smaller peaks at multiples of this period are found. If the simulation is continued, the distribution will continuously shift to the right with time.
For the top spray configuration a different picture is obtained (see Fig. 6). Since there is no directed flow profile as in the Wurster-coater, the particle trajectories are randomly

influenced by the high number of individual collisions in the fluidized bed. This leads to a wide residence time distribution of the particles in the spray zone, which corresponds to inhomogeneous wetting. Some particles spent up to 5 % of the simulation time inside the spray zone, whereas 30 % were not wetted at all.

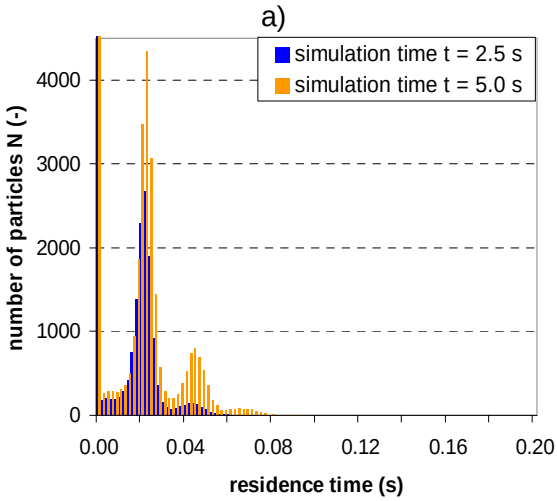

Fig. 5: Residence time distribution in the spray zone for the Wurster-coater.

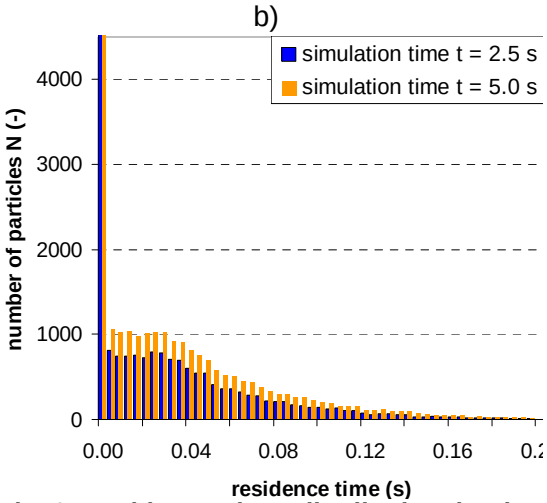

Fig. 6: Residence time distribution in the spray zone for the top-spray granulator.

Simulations including heat and mass transfer

Temperature and moisture content of the individual particles as well as temperature and humidity profiles of the gas phase in the apparatus can be calculated.
Initially all 10,000 particles are dry. Following the continuous liquid injection, more and more particles are wetted. Accordingly, the peak in Fig. 7 is shifted to the right with time. Due to inhomogeneous wetting, the particle moisture distribution gets broader. After 30 s simulation time the wetting/drying equilibrium is reached.

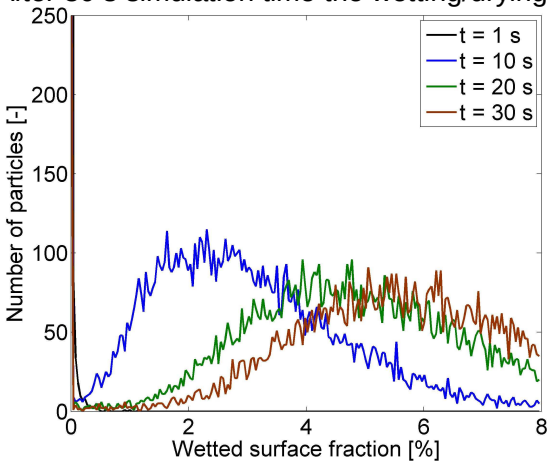

Fig. 7: Particle moisture distribution.

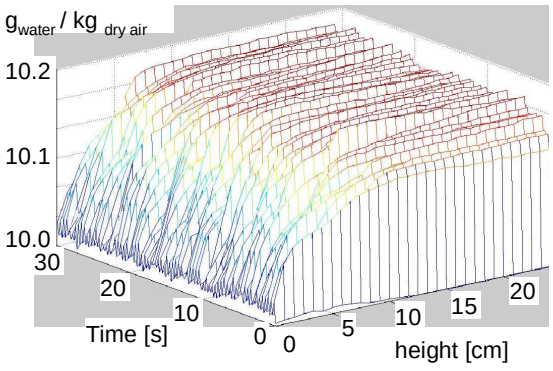

Fig. 8: Humidity profile of the gas phase.

In Fig. 8, the humidity of the gas phase is presented as a function of the height of the granulator and time. Due to evaporation, the humidity increases steeply with the height of the apparatus and slowly with time.

EXPERIMENTAL RESULTS

Experimentally the effect of different granulator configurations on the agglomeration behavior of spray dried glucose syrup in a fluidized bed (Glatt GCPG 3.1) was studied. The geometry of the fluidization chamber is the same in both cases, only the position of the nozzle was varied and the draft tube was inserted for the bottom spray case. Pure water was injected as binder and all operating conditions were kept constant.
While a narrow particle size distribution of the agglomerates is obtained with the Wurster-coater, the size distribution of the product from the top spray granulator is much broader. In the top spray granulator more oversize agglomerates are built. The experimental results of the particle size distribution (Fig. 9) correspond very well with the residence time distributions of the particles in the spray zone found in the numerical simulations (Figs. 5 and 6).

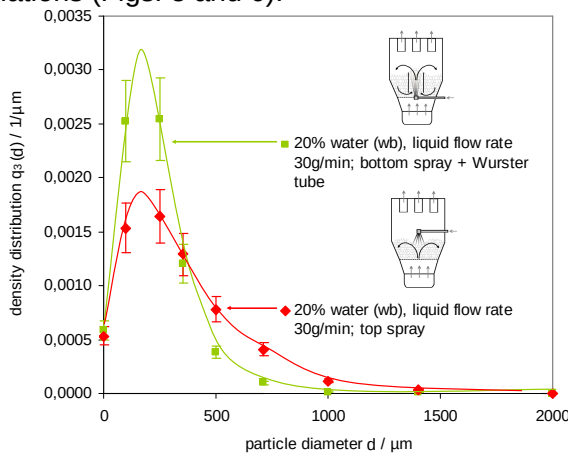

Fig. 9. Comparison of the agglomerate size distribution obtained in two different granulator configurations.

The simulations showed that the top spray configuration had an inhomogeneous residence time of the particles in the spray zone indicating unfavorable wetting.
This is reflected by the broad size distribution of the produced agglomerates. The Wurster-coater had a narrow residence time distribution, which matches well with the shape of the particle size distribution of the agglomerates.

CONCLUSIONS

For two different granulator configurations the homogeneity of the liquid distribution among the particle phase was investigated numerically on the scale of individual particles with the help of coupled DEM-CFD simulations. The residence time distribution of the particles in a conical spray zone at the tip of the injection nozzle allows estimating their moisture content. The results show that the Wurster-granulator is characterized by a narrow residence time distribution, whereas the top spray configuration leads to a wide residence time distribution. The positive effect of a Wurster tube on the distribution of the spray liquid seen in the DEM-CFD simulations was approved by agglomeration experiments. Coupled with heat and mass transfer relations, the DEM-CFD model

allows the direct calculation of the temperature and moisture content of the individual particles and the gas phase in a fluid bed granulator.

ACKNOWLEDGEMENT

We would like to thank Nestec S.A. for the financial support and Dr.-Ing. Michael Jacob from Glatt Ingenieurtechnik GmbH, Weimar for the supply of geometry data.

NOTATION

A	area	m^2	$\mathbf{n}$	normal unit vector	-
e	coefficient of restitution	-	p	pressure	Pa
E_{kin}	kinetic energy	J	Q	heat stream	W
$\mathbf{F}$	force	N	S_p	momentum sink term	$N\ m^{-3}$
$\mathbf{g}$	gravitation	$m\ s^{-2}$	t	time	s
H	enthalpy	J	$\mathbf{u}$	gas velocity	$m\ s^{-1}$
k	stiffness	$N\ m^{-1}$	$\mathbf{v}$	particle velocity	$m\ s^{-1}$
m	mass	kg	V	volume	m^3
$\dot{M}$	mass flow	$kg\ s^{-1}$	Y	gas moisture content	-
α	heat transfer coeff.	$Wm^{-2}K^{-1}$	ε	porosity	-
β	mass transfer coeff.	$m\ s^{-1}$	η	damping coefficient	Nsm^{-1}
$\beta_{g\text{-}p}$	momentum transfer coeff.	$kgm^{-3}s^{-1}$	ρ	density	$kg\ m^{-3}$
δ	displacement (overlap)	m	τ	gas phase stress tensor	Pa

REFERENCES

[1] Palzer, S.: Influence of material properties on the agglomeration of water-soluble amorphous particles. *Powder Technology* **189** (2), 2009, 318-326.
[2] Ergun, S.: Fluid flow through packed columns. *Chemical Engineering Progress* **48**, 1952, 89–94.
[3] Wen, Y.C. Yu, Y.H.: Mechanics of Fluidization. *Chemical Engineering Progress Symposium Series,* **62**, 100-111.[4] Hertz, H. Über die Berührung fester elastischer Körper. *Journal für die Reine und Angewandte Mathematik* **92**, 1882, pp. 156-171.
[5] Mindlin, R.D., Deresiewicz, H.: Elastic spheres in contact under varying oblique forces. *Transactions of ASME, Ser. E. J. of applied Mechanics* **20**, 1953, pp. 327-344.
[6] Tsuji, Y., Tanaka, T., Ishida, T.: Lagrangian numerical simulation of plug flow of cohesionless particles in a horizontal pipe. *Powder Technology* **71**, 1992, pp. 239-250.
[7] Antonyuk, S., Heinrich, S., Tomas, J., Deen, N.G., van Buijtenen, M.S. and J.A.M. Kuipers: Energy absorption during compression and impact of dry elastic-plastic spherical granules. *Granular Matter* **12** (1), 2010, pp. 15-47.
[8] Wurster, D. E.: Particle Coating Process. *U.S. Pat. No. 3253944,* May 31, 1966.